1

Iron-Catalyzed Radical Asymmetric Reactions

Yajun Li, Changqing Ye, and Hongli Bao

State Key Laboratory of Structural Chemistry, Key Laboratory of Coal to Ethylene Glycol and Its Related Technology, Center for Excellence in Molecular Synthesis, Fujian Institute of Research on the Structure of Matter, Chinese Academy of Sciences, Fuzhou, P. R. China

1.1 Introduction

The remarkable earth's abundance and low toxicity of iron make it an environmentally benign and economically viable alternative to conventional transition-metal catalysts. Over the past several decades, the development of iron-catalyzed reactions has exemplified the ingenuity and innovation within the organic chemistry community, and iron catalysis has become a cornerstone in modern organic synthesis, revolutionizing the way chemists construct complex molecules [1–9]. Harnessing the unique reactivity of iron, researchers have developed a diverse array of transformations that have not only expanded the synthetic toolbox but also addressed sustainability challenges in the field. From unconventional bond formations to intricate cascade reactions, iron catalysis has demonstrated exceptional versatility and efficiency, offering a promising platform for the continued advancement of sustainable synthetic methodologies.

Iron-catalyzed asymmetric reactions have garnered significant attention in the field of organic chemistry, with several excellent reviews documenting the remarkable progress achieved [10–18]. The development of chiral ligands and the elucidation of their role in controlling the enantioselectivity of iron-catalyzed reactions has been a key focus. Chiral porphyrins, chiral bipyridines, chiral salens, chiral bisoxazolines (BOX) and pyridine bisoxazolines (PyBOX), chiral diamines, chiral diphosphines, chiral binaphthyls, and planar-chiral ferrocenyls were among the most studied ligands for iron catalysis. The continuous exploration and refinement of iron-catalyzed asymmetric reactions showcase their potential as powerful tools in asymmetric synthesis. For example, iron-catalyzed enantioselective oxidation, hydride transfer, activation of Lewis basic substrates, carbene transfer, nitrene transfer, and more provide transformative strategies for accessing enantioenriched compounds sustainably.

Catalytic Asymmetric Radical Reactions, First Edition. Edited by Xin-Yuan Liu and Guosheng Liu.

In this chapter, we will introduce the advancements in iron-catalyzed radical asymmetric reactions. In this field, iron-porphyrins play an important role in biomimetic radical asymmetric catalysis. By using metalloporphyrins as the catalysts, researchers have been able to successfully mimic several types of reactions, including epoxidation [19–21], cyclopropanation [22–24], sulfoxidation [25–27], C—H amination/hydroxylation [28, 29], and so on. Several reviews on metalloporphyrin catalysis have been well documented to cover the remarkable achievements [30–39]. On the other hand, the Arnold group elegantly pioneered the use of P411-mutants derived from well-known cytochromes P450 in organic reactions. Their work has led to great successes in radical asymmetric C—H functionalization [40–50], cyclopropanation [51–58], and so on [59–69]. Important reviews on the reactions of P411-mutants and cytochromes P450 have been published [70–76]. Therefore, these are out of the scope of this chapter and will only be briefly depicted (Schemes 1.1 and 1.2).

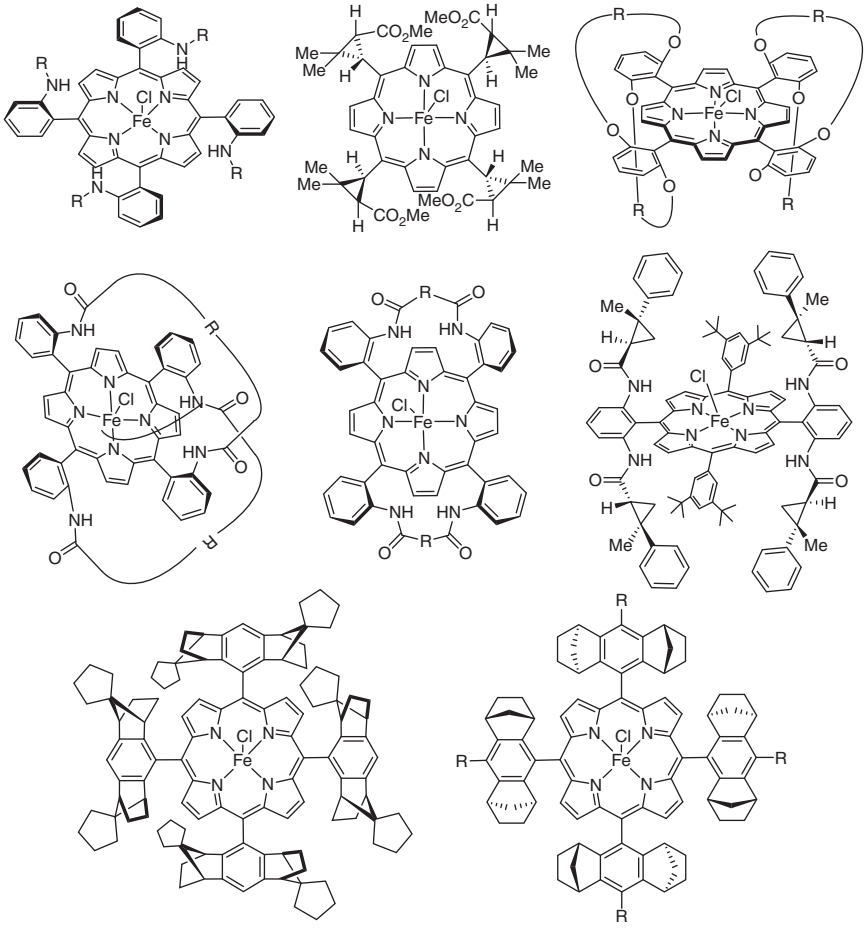

Scheme 1.1 Selected iron-porphyrins for radical asymmetric catalysis.

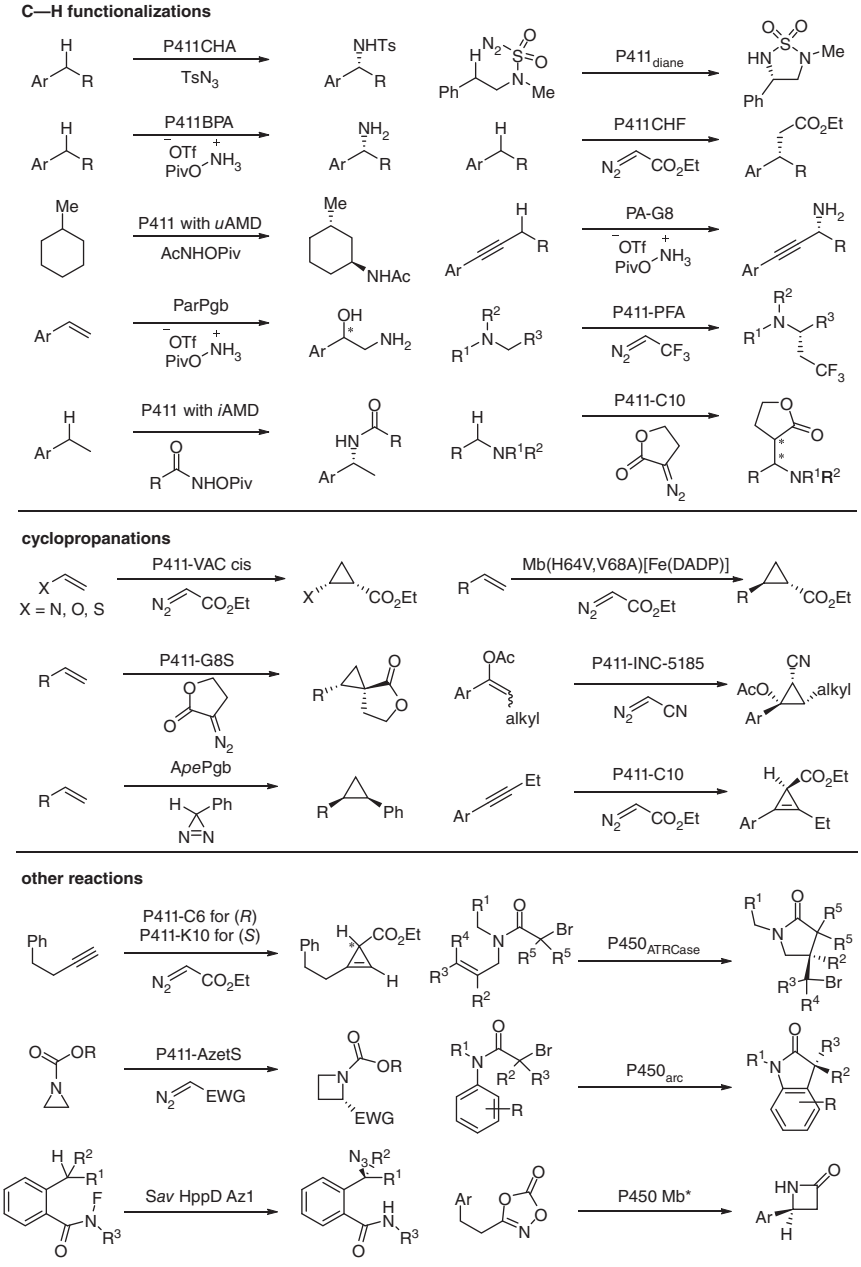

Scheme 1.2 Engineered cytochrome P450s for radical asymmetric catalysis.

Sibi and coworkers have made substantial contributions to the advancement of radical asymmetric chemistry and a comprehensive survey of the progress achieved in enantioselective radical reactions has recently been updated [77–79]. However, the utilization of iron/chiral ligand complexes in asymmetric radical

reactions is unexpectedly underdeveloped [80–87]. This may stem from two pivotal reasons: (i) the challenge in controlling the enantioselectivity of highly reactive radicals; (ii) iron's capacity to adopt various oxidation states and partake in a diverse range of radical-mediated elementary processes. This chapter aims to elucidate how asymmetry is controlled in iron-catalyzed radical asymmetric catalysis.

1.2 Asymmetric Oxidative Coupling of C—H Bonds

1.2.1 Coupling for Binaphthyl Synthesis

Transition-metal-mediated oxidative C—H/C—H coupling reactions represent one of the most straightforward and powerful tools in modern organic synthetic chemistry [88–90]. In 2010, Katsuki and coworkers pioneered the studies on iron-catalyzed radical asymmetric oxidative C—H/C—H coupling for the synthesis of C_1-symmetric 1,1′-bi-2,2′-naphthols (BINOLs) (Scheme 1.3) [91]. Using the

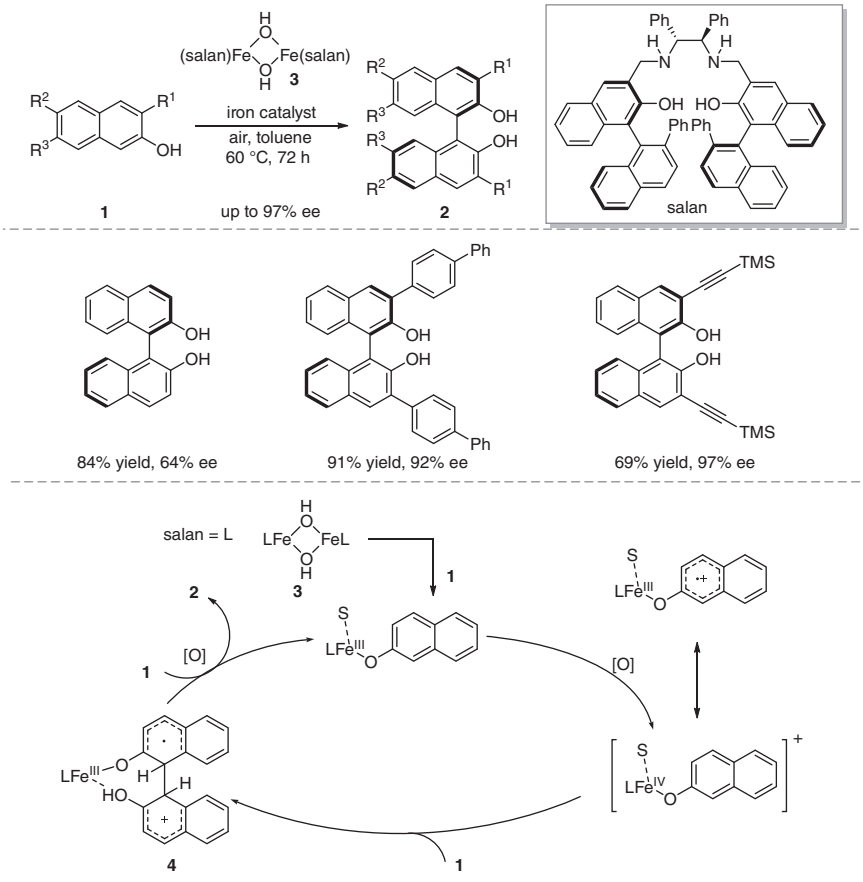

Scheme 1.3 Iron-catalyzed C—H/C—H cross-coupling of 2-naphthols.

iron(salan) complex as the catalyst, a range of 2-naphthols **1** underwent the aerobic oxidative cross-coupling reactions and many highly enantiopure BINOLs **2** can be obtained with up to 95% enantiomeric excess (ee). The mechanistic studies suggested that the (di-μ-hydroxo)iron^{III}(salan) catalyst **3** first underwent ligand exchange with a 2-naphthol **1** to form the 2-naphtholated iron^{III}(salan) species. The latter was oxidized to form the 2-naphtholated iron^{IV}(salan) species, which then asymmetrically reacted with another molecule of 2-naphthol **1** to give the radical cation species **4** that was associated with the iron^{III}(salan) core. After further oxidation and dissociation, the final chiral BINOL **2** was produced and the iron catalyst was recycled. The oxidation of 2-naphtholated iron^{III}(salan) to 2-naphtholated iron^{IV}(salan) species might be the rate-determining step of this iron-catalyzed oxidative coupling.

In 2016, the Pappo group disclosed that enantioselective oxidative homocoupling and cross-coupling of 2-naphthols can be catalyzed by chiral iron phosphate complexes **5** (Scheme 1.4) [92]. Enantioenriched C_1- and C_2-symmetric BINOLs can be smoothly produced in up to 92% ee. After reaction condition screening, the chiral phosphonic acid (CPA) with 4-^{t}Bu-Ph substituents was found to be the best chiral ligand. Di-*tert*-butyl peroxide (DTBP) was used as the oxidant and 1,2-dichloroethane (DCE)/1,1,1,3,3,3-hexafluoroisopropanol (HFIP) was used as the mixed solvent. Based on kinetic studies, an iron-catalyzed oxidative radical-anion coupling mechanism was proposed. They point out that the use of CPAs as ligands may provide a general platform for the application of chiral iron catalysts in asymmetric synthesis.

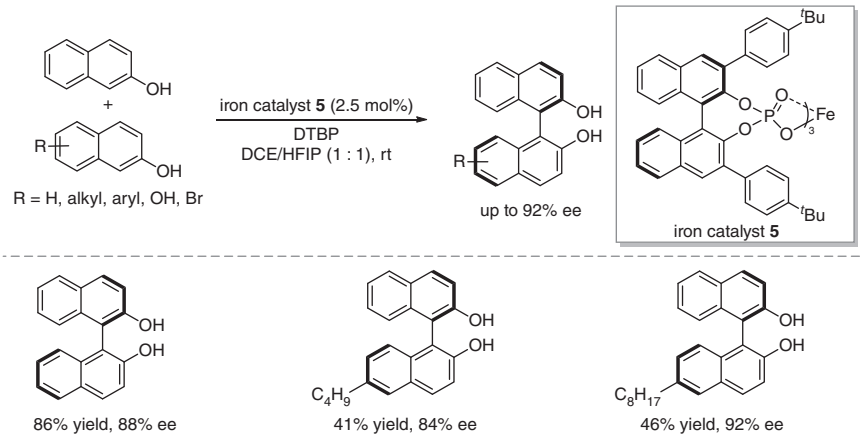

Scheme 1.4 Iron-catalyzed C–H/C–H cross-coupling of 2-naphthols.

Bryliakov and coworkers tested a series of bipyrrolidine-derived iron aminopyridine complexes as the catalysts in the oxidative homocoupling of 2-naphthols [93]. However, when the reaction was carried out in chlorobenzene at 50 °C, only up to 56% ee was obtained. While the Ishihara group reported a chiral diphosphine oxide–iron(II) complexes ((*S*)-xylyl-^{i}PrO-BIPHEP-oxide: $Fe(OTf)_2$) for oxidative

homocoupling of 2-naphthols with *tert*-butyl hydroperoxide (TBHP) as the oxidant. The C_1-symmetric BINOLs were generated in up to 98% yield and 92% ee [94].

2-Amino-2′-hydroxy-1,1′-binaphthyls (NOBINs), as a kind of biaryl compounds bearing axial chirality, frequently serve as building blocks, ligands, or catalysts in asymmetric transformations [95]. In 2022, Pappo and coworkers developed an interesting asymmetric oxidative C—H/C—H cross-coupling between 2-naphthols and 2-aminonaphthalene derivatives **6** (Scheme 1.5) [96]. This cross-coupling reaction was catalyzed by a novel type of chiral redox disulfonate iron complex $[Fe((R_a)\text{-BINSate})]^+$ (BINSate = 1,1′-binaphthalene-2,2′-disulfonate), which was in situ generated from iron salt and (*Ra*)-BINSA **8**. Under the optimal reaction conditions with lauroyl peroxide (LPO) as the oxidant and boron-trifluoride-etherate $BF_3 \cdot OEt_2$ as the additive, the selective cross-coupling reactions proceeded smoothly, providing the NOBINs **7** in good yields and high enantioselectivities.

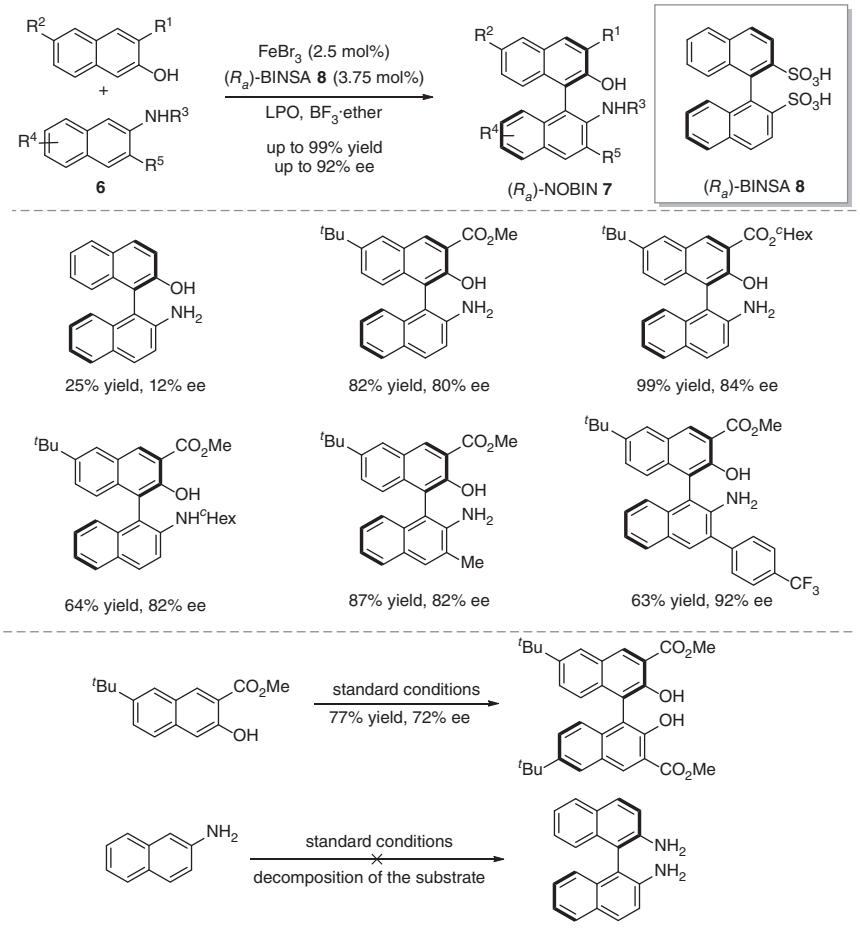

Scheme 1.5 Iron-catalyzed C—H/C—H cross-coupling of 2-naphthols and 2-aminonaphthalene derivatives.

Without $BF_3 \cdot OEt_2$, the [Fe((R_a)-BINSate)]$^+$ complex would catalyze the oxidative homocoupling of a 2-naphthol derivative to afford the corresponding BINOL as the product, while the homocoupling of 2-aminonaphthalene led to the complete decomposition of the substrate. These results suggested that a radical–nucleophile coupling mechanism was involved. Moreover, the high-resolution mass spectrometry (HRMS) study and the nonlinear effect experiment suggested the involvement of mono-ligand/mono-iron species during the selectivity-determining step.

The Knölker group found that the iron/CPA complex enabled the asymmetric C—H/C—H coupling of 2-aminonaphthalene derivatives (Scheme 1.6) [97]. After examination of more than 10 different chiral phosphonic acids, it was found that the use of triphenylsilylated CPA **10** afforded the best result. The coupled 2,2′-bis(arylamino)-1,1′-biaryls **9** can be obtained in up to 97% yield and 90% ee. However, the enantioselectivity was poor for most substrates. Notably, higher yields can be obtained for phenyl naphthyl amines, and heavily electron-rich substituents are required for diphenyl amines to afford better yields and chemoselectivity. A similar mechanism proceeding via a radical cation-chiral phosphate ion pair was proposed.

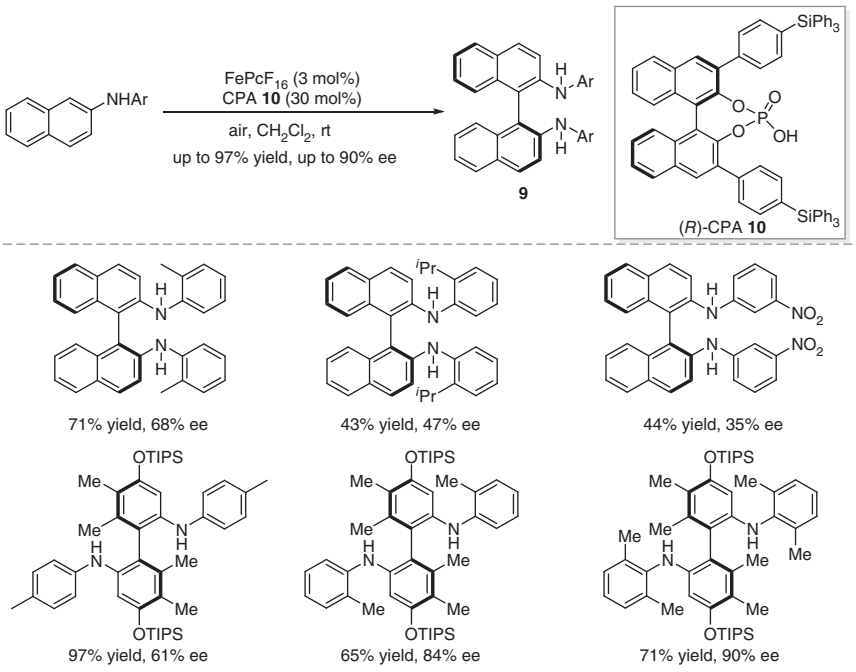

Scheme 1.6 Iron-catalyzed homocoupling of 2-aminonaphthalene derivatives.

1.2.2 Coupling of Other C–H Bonds

In 2012, the Katsuki group found that if the 1-position of 2-naphthol was blocked by a substituent, these 2-naphthols would react with nitroalkanes **11** to

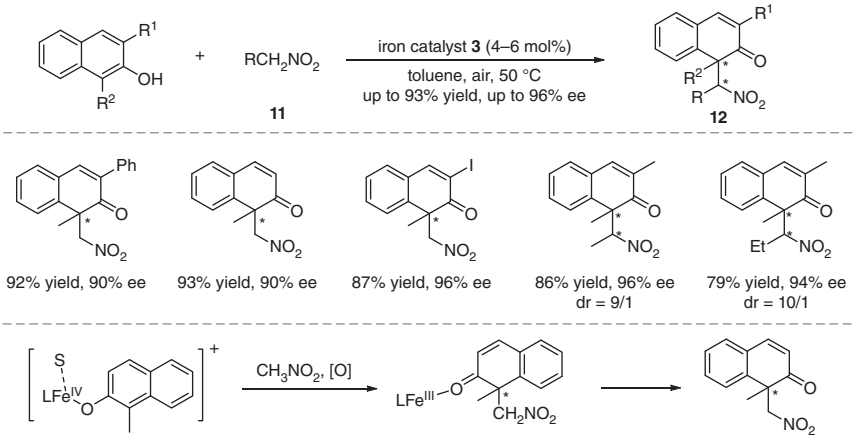

Scheme 1.7 Iron-catalyzed coupling of 2-naphthols and nitroalkanes.

generate the enantioenriched products with an all-carbon quaternary stereocenter (Scheme 1.7) [98]. In the presence of the previously discussed iron(salan) complex **3** as the catalyst, the reactions simultaneously underwent oxidative dearomatization/asymmetric construction of the all-carbon quaternary stereocenter in an intermolecular manner to produce the products **12** in up to 93% yield and 96% ee. This iron(salan) complex-catalyzed asymmetric aerobic oxidative coupling of 2-naphthols and nitroalkanes was supposed to involve the nucleophilic attack of the nitroalkane to the radical cation species.

Pappo and coworkers explored the asymmetric cross-dehydrogenative coupling of 2-naphthols with β-ketoester derivatives (Scheme 1.8) [99]. At room temperature, the chiral iron phosphate catalyst derived from iron salt and ligand **15** and DTBP in a mixed solvent of $PhCF_3$/HFIP would only result in the homocoupling of 2-naphthols. Interestingly, the coupling of 2-naphthols with β-ketoester derivatives

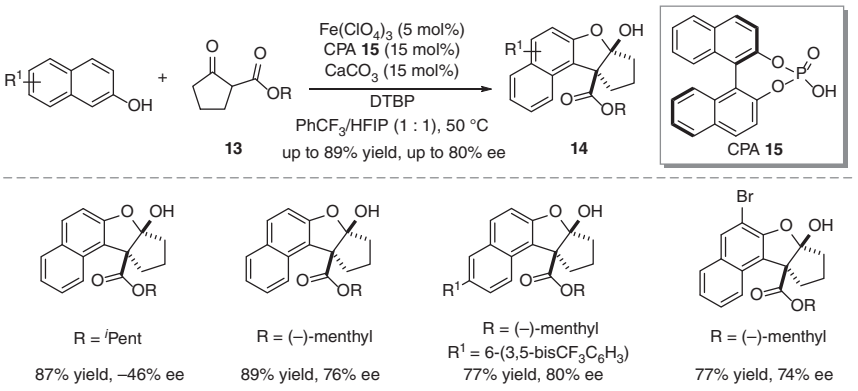

Scheme 1.8 Iron-catalyzed cross-coupling of 2-naphthols and β-ketoester derivatives.

13 proceeds smoothly at elevated temperatures, yielding the corresponding polycyclic hemiacetals **14** in good yields. Extensive screening of CPA ligands revealed a correlation between the size of the 3,3′-substituents of the phosphoric acid and the diastereoselectivity of the product. Notably, the use of chiral auxiliary (−)-menthyl was found to be crucial for enantiocontrol. The mechanism studies supported that the coupling took place between two associated ligands via a radical–anion coupling mechanism.

The significance and interest in heterobiaryl compounds with axial chirality have been growing across various fields. However, the enantioselective synthesis of these compounds through direct oxidative methods remains a significant challenge. In 2022, Smith and coworkers developed an iron-catalyzed oxidative cross-coupling of 2-naphthols and NH-free indoles for the synthesis of atropisomeric heterobiaryl compounds (Scheme 1.9) [100]. The chiral PyBOX ligand **18** was found to be the best one, and the cross-coupling product **17** can be obtained with high levels of chemoselectivity and enantioselectivity. The measurement of the oxidation potentials of 2-tert-butylindole and 2-isopropylphenyl 3-hydroxy-2-naphthoate clearly showed that the indole exhibited a lower oxidation potential compared to the

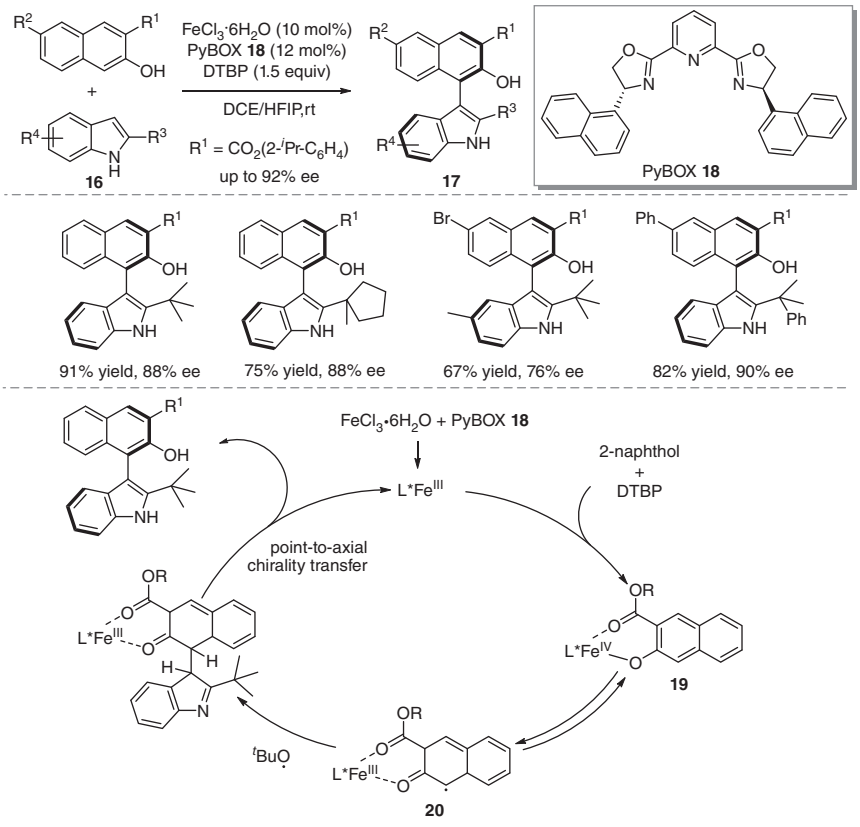

Scheme 1.9 Iron-catalyzed cross-coupling of 2-naphthols and indoles.

naphthol component under standard conditions. Interestingly, the cross-coupling of 2-naphthols and NH-free indoles **16** was found to exclusively produce the cross-coupled products **17** without any competing homocoupling products. These findings suggest that the oxidation of the heterocyclic component does not significantly contribute to the catalytic cycle. Further mechanistic investigations, including radical clock experiment, HRMS, electron paramagnetic resonance (EPR) spectroscopy, and the Hammett plot analysis, supported the radical-involved mechanism.

First, the PyBOX ligand associated with the Fe(III) salt to form an octahedral Fe/PyBOX complex, which underwent ligand exchange with the 2-naphthol to produce a complex with the 2-naphthol binding in a bidentate fashion. Second, the single-electron transfer of the Fe(III) complex by DTBP afforded an Fe(IV) complex **19** and an accompanying *tert*-butoxy radical, and the subsequent reversible single-electron transfer generates the Fe(III)-ligated naphthoxy radical **20**. Then, directly controlled by the chiral ligand, the π-nucleophilic indole could facially attack the Fe(III)-ligated naphthoxy radical via an outer-sphere mechanism in the presence of the *tert*-butoxy radical to afford the coupling product, followed by ligand exchange to enable release of the enantioenriched heterobiaryl and an Fe(III) complex for the next catalytic cycle.

The previous work covers dehydrogenative coupling in which at least one sp^2-hybridized carbon was involved. The cross-dehydrogenative coupling of two inert C(sp^3)—H bonds would generate two adjacent sp^3-hybridized carbons [101, 102]. In 2024, Feng, Liu, and coworkers reported an iron-catalyzed radical asymmetric dehydrogenative coupling of 2-acylimidazoles **21** with benzylic and allylic hydrocarbons as well as nonactivated alkanes **22** (Scheme 1.10) [103]. In this

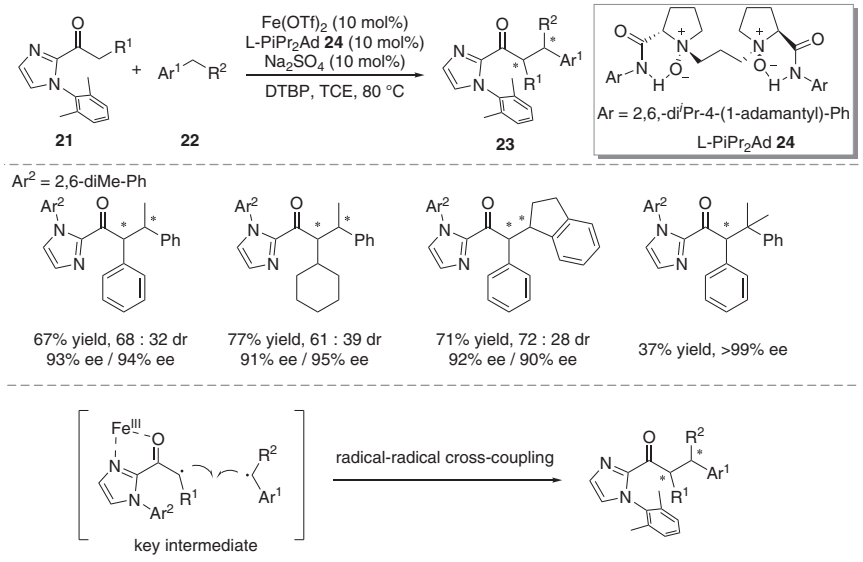

Scheme 1.10 Iron-catalyzed coupling of two inert C(sp^3)—H bonds.

method, the two inert C(sp^3)—H bonds were enantioselectively coupled. The readily available and tunable *N*,*N*′-dioxide ligand L-PiPr$_2$Ad **24** and DTBP exhibited excellent asymmetric induction. Based on the Density functional theory (DFT) calculation and control experiments, a radical-radical cross-coupling mechanism was proposed.

1.3 Asymmetric C—C Coupling of Alkyl Halides

The Kumada reaction is a widely employed method in organic synthesis, which involves the cross-coupling of an organohalide with an organometallic compound. In 2015, the Nakamura group developed the first iron-catalyzed asymmetric Kumada reaction (Scheme 1.11) [104]. The enantioselective cross-coupling of α-haloesters **25** with aryl Grignard reagents **26** was conducted in the presence of Fe(acac)$_3$/chiral biphosphine ligand **28**. Good yields and high ee values of the coupled products **27** were obtained. Deprotection of the coupled products led to carboxylic acids, and further co-crystallization with octylamine constituted a nice approach for the synthesis of enantiopure dexibuprofen **29**. As supported by the control experiments, the reaction involved the abstraction of a halogen

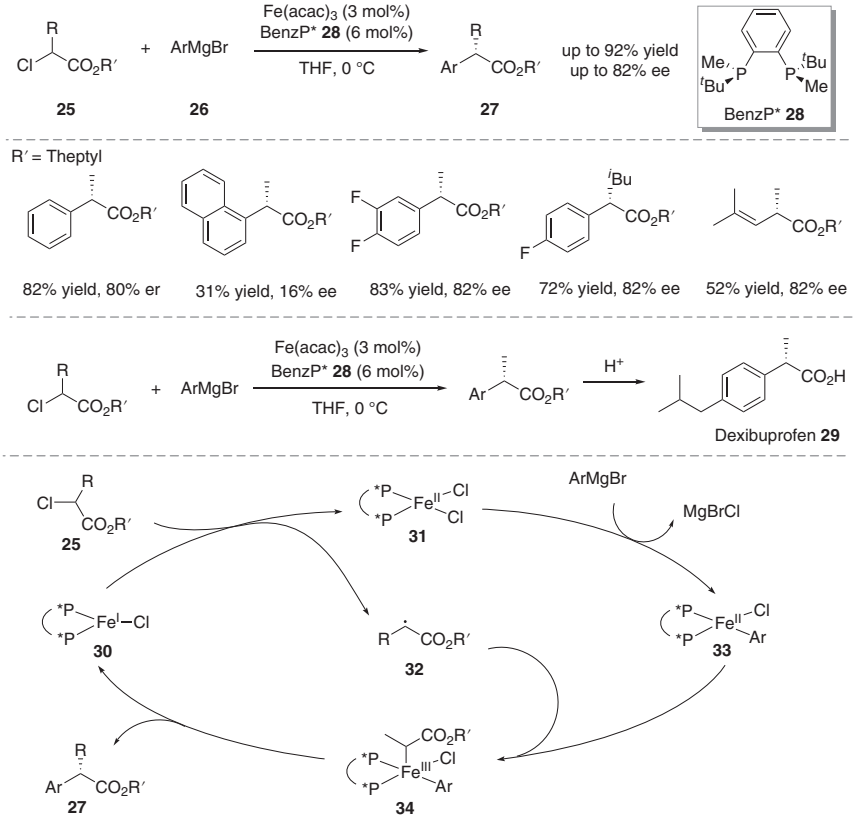

Scheme 1.11 Iron-catalyzed asymmetric Kumada reaction.

from α-haloesters to generate an alkyl radical intermediate and underwent a Fe(III)—Fe(II)—Fe(I) catalytic cycle.

Shortly after that, the authors conducted theoretical calculations to further investigate the mechanism [105]. It was found that Fe^{I}(BenzP*)Cl complex **30** was the active intermediate for the C—Cl bond activation to provide L*$Fe^{II}Cl_2$ **31** and an alkyl radical **32**. The formation of the C—C bond through an inner-sphere mechanism was the selectivity-determining step. Transmetalation of the L*$Fe^{II}Cl_2$ **31** with aryl Grignard reagent generated a L*ArFe^{II}Cl species **33**, which bonded with the alkyl radical **32** to afford a L*Fe^{III} species **34**. The reductive elimination afforded the coupling product **27** and regenerated the L*Fe^{I}Cl complex **30** that enabled the halogen atom abstraction process. The theoretical study provided important mechanistic insights into the iron-catalyzed cross-coupling reactions and is very important for the development of iron-based catalysts for highly stereoselective synthetic organic transformations. At the same time, Gutierrez and coworkers have also performed DFT studies on this iron-catalyzed Kumada coupling and further supported the proposed mechanism [106].

In 2023, Gutierrez and coworkers reported an iron-catalyzed enantioselective three-component coupling reaction (Scheme 1.12) [107]. In the presence of $Fe(acac)_3$/BenzP* as the catalytic system, the cross-couplings of vinyl boronates **35**, (fluoro)alkyl halides **36**, and Grignard reagents reacted well to produce the enantioenriched boro-products, which were transferred into the corresponding chiral alcohols **37** with high efficiency. The α-boryl radicals **38** generated from the addition of alkyl radicals to vinyl boronates was supposed to be involved.

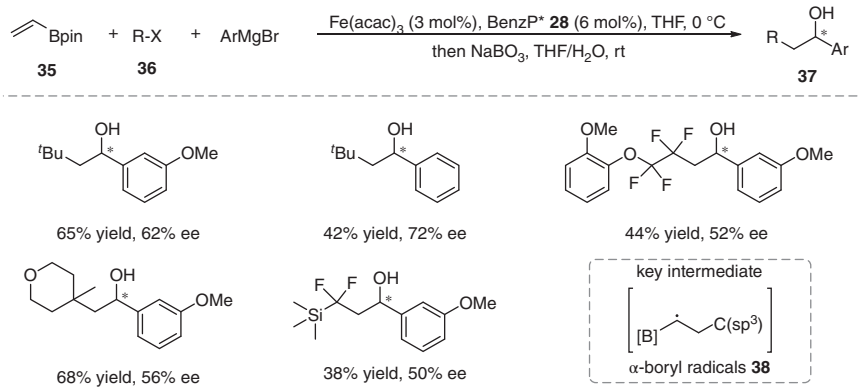

Scheme 1.12 Iron-catalyzed radical asymmetric three-component coupling.

In 2019, the Nakamura group reported an iron-catalyzed Suzuki–Miyaura coupling reaction (Scheme 1.13) [108]. In the presence of catalytic amounts of $FeCl_2$ and (*R*,*R*)-QuinoxP* **41**, the cross-coupling of *tert*-butyl α-bromopropionate **39** and lithium arylborates **40** took place to afford various optically active α-arylpropionic acids after cascade hydrolysis.

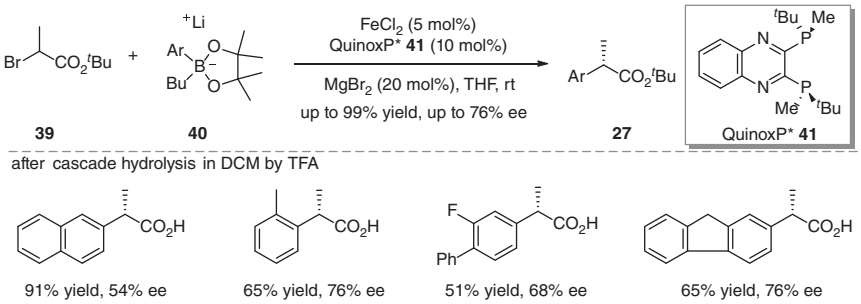

Scheme 1.13 Iron-catalyzed asymmetric Suzuki–Miyaura coupling.

1.4 Asymmetric C—N Bond Formation

The C—N bond is one of the most common chemical bonds found in both natural and synthetic molecules. Numerous naturally occurring organic compounds, pharmaceuticals, agrochemicals, and functional materials include at least one nitrogen atom, highlighting the widespread importance of this bond in various fields. The Xu group made preliminary attempts at iron-catalyzed radical asymmetric C—N bond formation [109, 110]. The use of $Fe(NTf_2)_2$/chiral BOX ligand induced the enantioselectivity. Both of the (*E*)- and (*Z*)-olefins with a functionalized hydroxylamine were transferred into *syn*-hydroxyl oxazolidinone with the same ee and dr (82% ee, dr > 20 : 1), which suggested a radical mechanism.

In 2020, Bao and coworkers reported the pioneering achievement of the first radical asymmetric carboazidation, a significant milestone even in light of notable advancements in achiral carboazidation reactions (Scheme 1.14) [111]. The catalytic complex was composed of $Fe(OTf)_2$ and Haixi-BOX ligand **45**. Many inexpensive industrial chemical feedstocks, including styrenes **42**, alkyl halides, fluoroalkyl halides, and $TMSN_3$ **43**, are viable substrates for the iron-catalyzed radical asymmetric carboazidation of olefins, with LPO serving as a radical initiator. Mechanistic studies revealed that this process involved the generation of a carbon radical, and the reaction may undergo a group transfer mechanism. It was supposed that the stereocontrol at the radical center was achieved through the synergistic effects of van der Waals and π interactions in the rigid chiral space created by the tridentate chiral NON-pincer ligand and iron. The generated chiral organoazides **44** can be transferred into valuable chiral primary amines, chiral phosphoramides, chiral benzylic 1,2,4-triazin-5(4*H*)-ones, chiral triazoles, and so on. The incorporation of natural product moieties, such as an estradiol derivative or a botulin derivative, emphasized the utility of this method. Furthermore, the obtained (*S*)-3-amino-3-phenylpropanoic acid through simple transformations served as a key intermediate for the synthesis of the anti-HIV drug Maraviroc.

Based on the mechanistic studies and DFT calculations, a catalytic cycle was proposed (Scheme 1.15). Upon ligand exchange with $TMSN_3$ **43**, the ligated Fe^{II} complex **46** would be transferred into the azido Fe^{II} species **47**. Then, a single-electron transfer (SET) process occurred between **47** and LPO to afford the crucial iron(III) azide

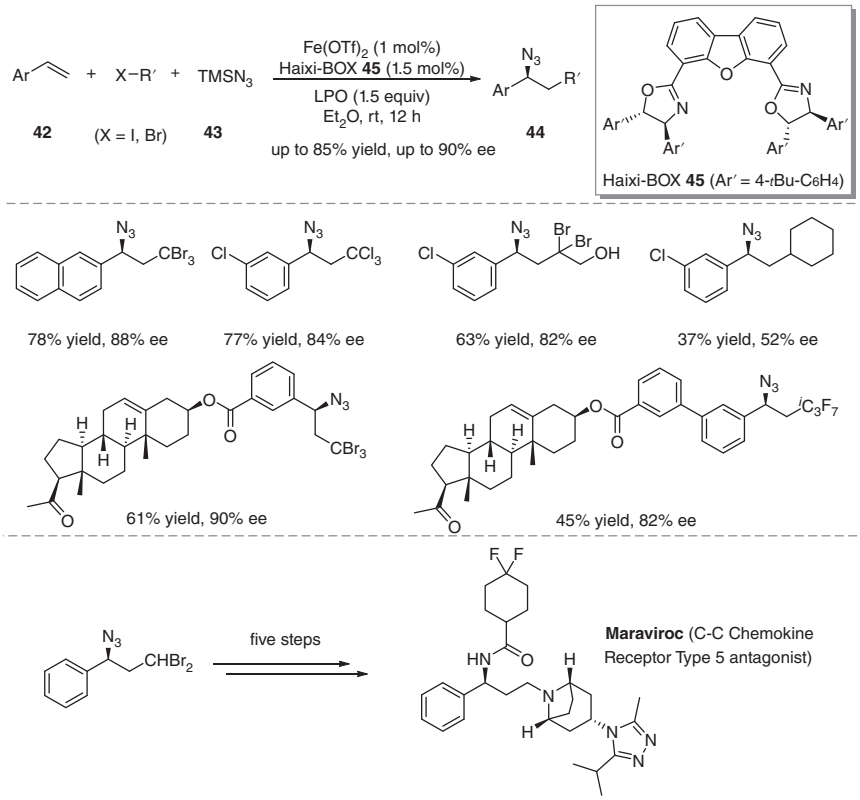

Scheme 1.14 Iron-catalyzed radical asymmetric carboazidation of styrenes.

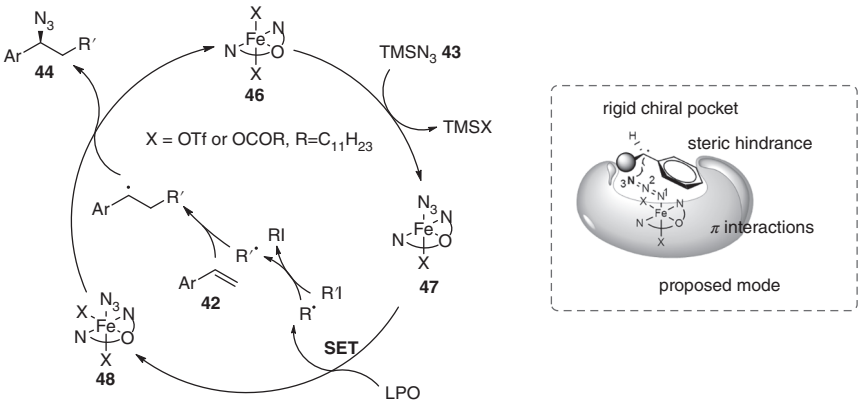

Scheme 1.15 The mechanism for iron-catalyzed radical asymmetric carboazidation.

species **48** and an alkyl radical R. Meanwhile, the alkyl radical abstracted the iodine atom from the (fluoro)alkyl iodide to form the fluoroalkyl radical R′, which was then added to a styrene to generate a benzylic radical **49**. The interaction between the iron(III) azide species **48** and the benzylic radical **49** led to the final product **44**.

Notably, the outer-sphere group transfer of the azido functionality was anticipated to occur on the N3-position, as depicted in Scheme 1.15.

Shortly thereafter, the Bao group expanded on their work by achieving an iron-catalyzed intermolecular asymmetric diazidation of di- or tri-substituted styrenes (Scheme 1.16) [112]. This advancement enabled the synthesis of a range of chiral diazidation products **50** that were previously inaccessible, which are essential for the generation of various nitrogen-containing compounds. Mechanistic studies suggest that the reaction proceeds via a radical pathway, wherein the stereocontrol of an acyclic radical is potentially achieved through a group transfer mechanism.

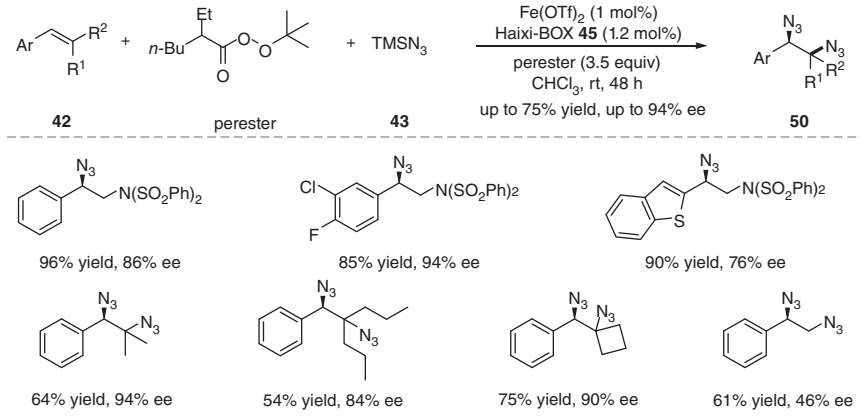

Scheme 1.16 Iron-catalyzed asymmetric aminoazidation and diazidation of styrenes.

In 2021, the Bao group developed an iron-catalyzed asymmetric azidation of benzylic peresters using $TMSN_3$ **43** (Scheme 1.17) [113]. The chiral Haixi-BOX

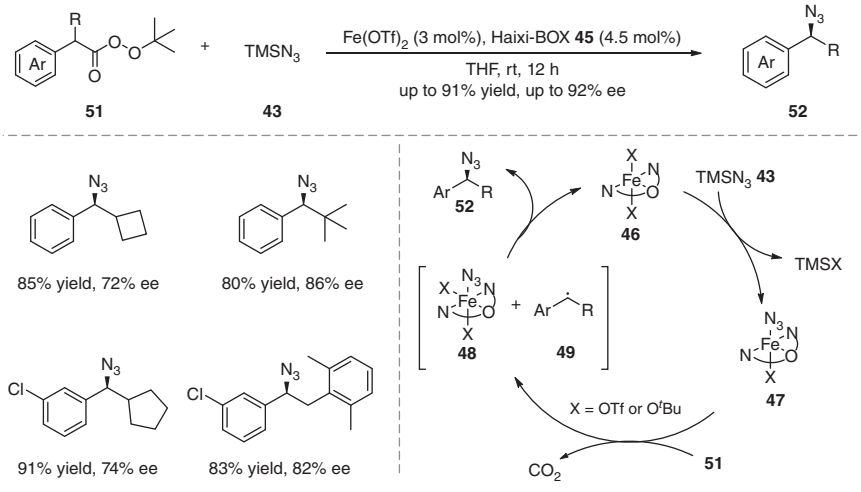

Scheme 1.17 Iron-catalyzed asymmetric azidation of benzyl peresters.

ligand **45** showed superior performance in this process. Various benzylic peresters **51** exhibited excellent reactivity, yielding enantioenriched azides **52** with high yields and good enantioselectivities under mild reaction conditions. Notably, the generated hydrocarbon radicals lack strong interactions. The resulting chiral benzyl azides **52** can be utilized in click reactions, phosphoramidation, and reductive amination reactions. The exchange of ligand between the L*Fe(II) species **46** and $TMSN_3$ **43** produced the L*Fe(II)-azide species **47**, which then underwent SET with the perester **51** to generate the L*Fe(III)-azide species **48** and the resulting benzylic radical **49**. An outer-sphere group transfer led to the formation of the final product **52** and the active catalyst **46**.

In 2021, Feng and coworkers disclosed an $Fe(OTf)_2$/chiral *N*,*N*′-dioxide complex-catalyzed radical enantioselective carboazidation and diazidation of α,β-unsaturated ketones and amides (Scheme 1.18) [114]. Alkyl peroxides **54**, Togni's reagent **55**, fluoroalkyl halides, and $TMSN_3$ **43** were well tolerated under the mild reaction conditions, and many substituted alkenes **53** were sequentially converted into α-azido carbonyl derivatives **56** with high enantioselectivity. Mechanistic studies and DFT calculations suggest that a radical pathway was involved and the azido transferred to the radical intermediate via an intramolecular five-membered transition state with the internal nitrogen of the Fe—N_3 species. A wide array

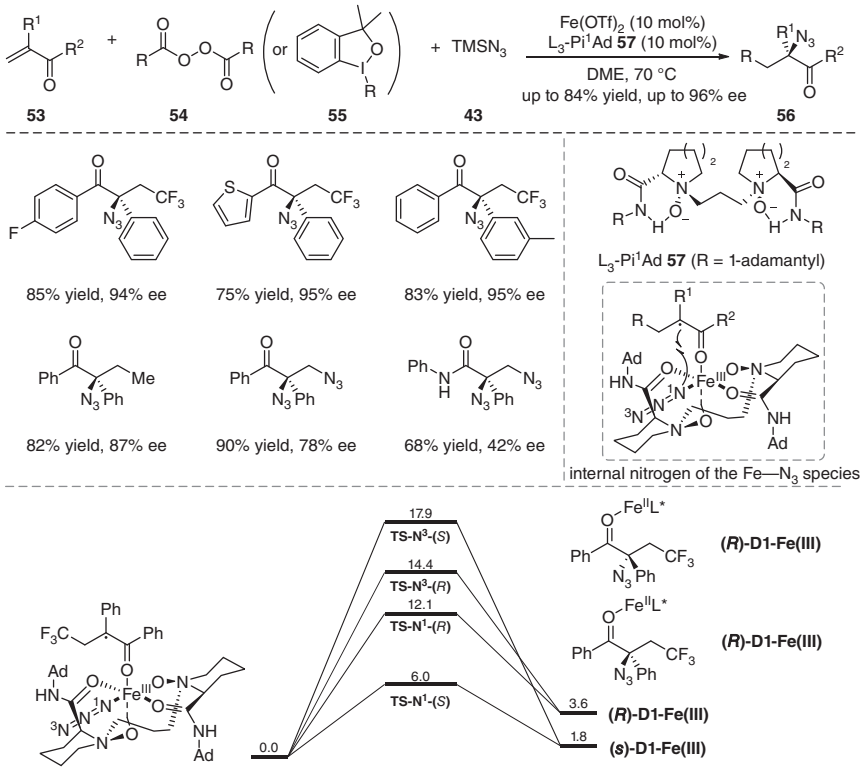

Scheme 1.18 Iron-catalyzed asymmetric azidation of alkenes.

of chiral α-azido carbonyl derivatives, which could be further transformed into highly valuable chiral amino ketones, amino alcohols, and vicinal diamines, were synthesized by this efficient protocol.

In 2023, Wang and coworkers developed an enantioselective radical decarbonylative azidation (Scheme 1.19, top) [115]. Catalyzed by the complex of Fe^{II}/BOX, various aldehydes **58** underwent radical decarbonylation to generate the benzyl radicals, which abstracted the azido group from the azido-Fe species to produce the enantioenriched azides **59**. Notably, *tert*-butylperoxybenzoate (TBPB) served as the radical initiator. The Lian group established an iron-catalyzed approach for the enantioselective synthesis of chiral β-azido sulfones (Scheme 1.19, bottom) [116]. SOgen: tetrabromothiophene S,S-dioxide **63** was selected as the sulfur dioxide source. A series of BOX ligands have been evaluated. The iron-catalyzed four-component reactions afforded the corresponding heavily functionalized azides **64** in good yields and high enantioselectivity.

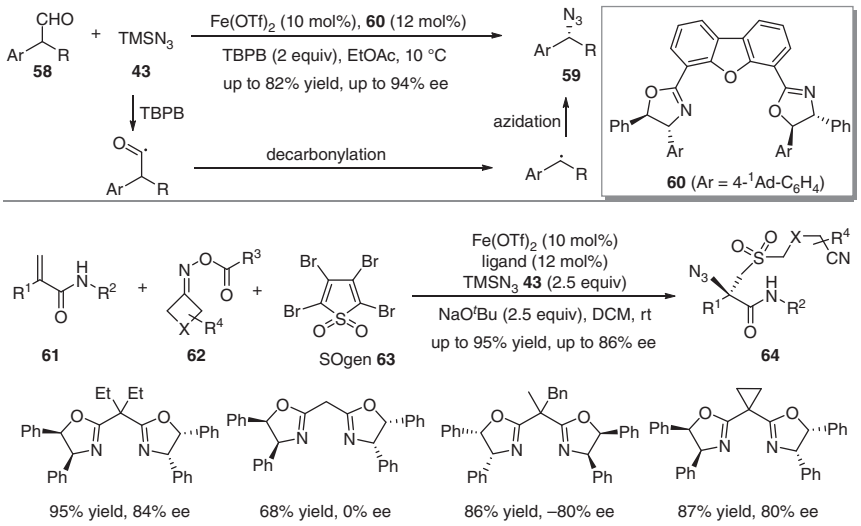

Scheme 1.19 Iron-catalyzed decarbonylative azidation and four-component reactions.

In 2008, the Bolm group made preliminary attempts on iron-catalyzed radical asymmetric aziridination of alkenes. The PyBOX ligand offered the synthetically valuable aziridine with moderate ee [117]. The Meggers group developed a Fe/tetradentate N4-ligand-catalyzed asymmetric ring contraction of isoxazoles **65** to 2*H*-azirines **66** (Scheme 1.20, top) [118]. They can be easily transferred into chiral aziridine, α-methyl phenylalanine ester, β-hydroxy and β-methoxy phenylalanine derivatives. Mechanistic studies revealed that heterolytic cleavage of the N—O bond induced by SET from the iron center and stereocontrolled C—N bond formation via intramolecular radical addition were found to be crucial. Very closely, Meggers and coworkers reported a ring construction of *N*-aroyloxyureas to form chiral 2-imidazolidinones **68** in up to 99% yield and with up to 95% ee (Scheme 1.20,

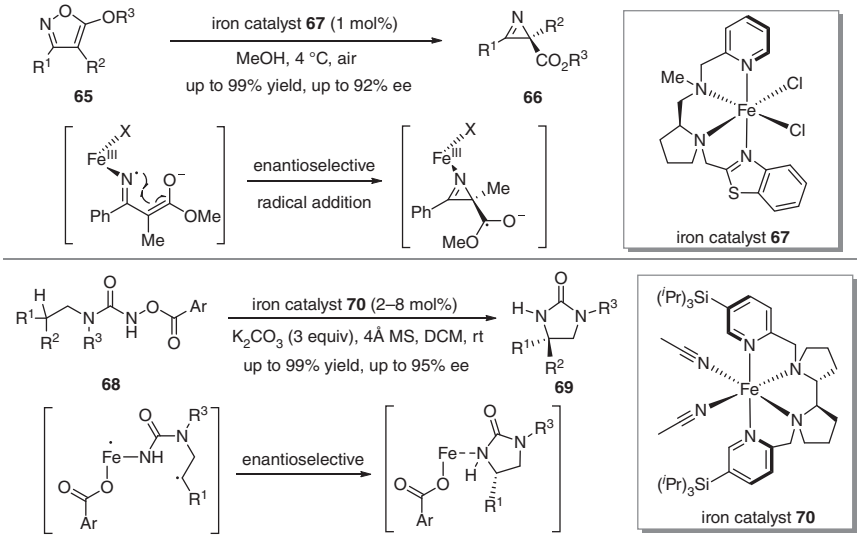

Scheme 1.20 Iron-catalyzed asymmetric radical ring contraction and C—H amination.

bottom) [119]. This iron-catalyzed enantioselective C(sp^3)—H amination facilitated the rapid construction of chiral nitrogen-containing heterocycles **69**, which can be hydrolyzed to yield valuable chiral vicinal diamines in a single step. Mechanistic studies suggested that the C—N bond formation step was enantioselectively controlled by the chiral iron complex.

1.5 Conclusion

This chapter compiles the advancements in iron-catalyzed radical asymmetric reactions. Stemming from Groves' pioneering work on catalytic radical asymmetric epoxidations facilitated by chiral iron-porphyrins, considerable progress has been made, predominantly in porphyrin-based biomimetic asymmetric catalysis. In consideration of the ongoing demand for new, economical, and sustainable reactions, recent years have witnessed advancements in chiral iron catalysis employing non-porphyrin-based ligands. A diverse array of chiral ligands, including chiral oxazolines, bidentate chiral phosphines, chiral phosphoric acids, chiral salens, chiral C_2 symmetric *N*,*N*′-dioxide ligands, and chiral bipyridines, have proven to be exceptional chiral auxiliaries, ensuring high levels of asymmetric induction in the field. By using these ligands, a wide range of noteworthy reactions extending beyond traditional epoxidations and cyclopropanations have been successfully achieved, facilitating enantioconvergent and sustainable construction of chiral C—C, C—N, C—O, and C—X bonds. Detailed insights into the catalytic models and mechanisms underpinning these radical asymmetric reactions are provided. Notably, great successes in enzymatic radical asymmetric synthesis should also be highly commended.

Despite the current ground-breaking developments that demonstrate the significance of iron-catalyzed radical asymmetric synthesis, this field remains underdeveloped, and many challenges need to be well addressed. First, the scope of reaction types is still narrow. Efforts should focus on exploring more efficient catalytic asymmetric transformations, particularly those that emulate natural processes. Second, there is a critical requirement for the design of new categories of chiral ligands that can expand the portfolio of this field. Third, more comprehensive understandings of the catalytic mechanism employed in iron catalysis would be vital for revealing the essence of enantiocontrol. It is evident that iron catalysis will continue to be a prominent topic in the forthcoming years. The pursuit of cost-effective, sustainable, and enantioselective methods is pivotal for the evolution of future organic synthetic chemistry.

References

1 Bolm, C., Legros, J., Le Paih, J., and Zani, L. (2004). *Chem. Rev.* 104: 6217–6254.
2 Díaz, D.D., Miranda, P.O., Padrón, J.I., and Martín, V.S. (2006). *Curr. Org. Chem.* 10: 457–476.
3 Bauer, E.B. (2015). *Top. Organomet. Chem.* 50: 1–18.
4 Bauer, I. and Knolker, H.J. (2015). *Chem. Rev.* 115: 3170–3387.
5 Furstner, A. (2016). *ACS Cent. Sci.* 2: 778–789.
6 Bauer, E.B. (2017). *Isr. J. Chem.* 57: 1131–1150.
7 Fang, G.-C., Cheng, Y.-F., Yu, Z.-L. et al. (2019). *Top. Curr. Chem.* 377: 23.
8 Rana, S., Biswas, J.P., Paul, S. et al. (2021). *Chem. Soc. Rev.* 50: 243–472.
9 Liu, Y., Shing, K.-P., Lo, V.K.-Y., and Che, C.-M. (2023). *ACS Catal.* 13: 1103–1124.
10 Gopalaiah, K. (2013). *Chem. Rev.* 113: 3248–3296.
11 Srour, H., Le Maux, P., Chevance, S., and Simonneaux, G. (2013). *Coord. Chem. Rev.* 257: 3030–3050.
12 Ollevier, T. and Keipour, H. (2015). *Top. Organomet. Chem.* 50: 259–309.
13 Ollevier, T. (2016). Catal. *Sci. Technol.* 6: 41–48.
14 Loup, J., Dhawa, U., Pesciaioli, F. et al. (2019). *Angew. Chem. Int. Ed.* 58: 12803–12818.
15 Pellissier, H. (2019). *Coord. Chem. Rev.* 386: 1–31.
16 Achar, T.K., Maiti, S., Jana, S., and Maiti, D. (2020). *ACS Catal.* 10: 13748–13793.
17 Casnati, A., Lanzi, M., and Cera, G. (2020). *Molecules* 25: 3889.
18 Liu, Y., You, T., Wang, H.-X. et al. (2020). *Chem. Soc. Rev.* 49: 5310–5358.
19 Groves, J.T. and Myers, R.S. (1983). *J. Am. Chem. Soc.* 105: 5791–5796.
20 Collman, J.P., Zhang, X., Lee, V.J. et al. (1993). *Science* 261: 1404–1411.
21 Collman, J.P., Wang, Z., Straumanis, A. et al. (1998). *J. Am. Chem. Soc.* 121: 460–461.
22 Mansuy, D., Battioni, P., Renaud, J.P., and Guerin, P. (1985). *J. Chem. Soc. Chem. Commun.* 155–156.

23 Gross, Z., Galili, N., and Simkhovich, L. (1999). *Tetrahedron Lett.* 40: 1571–1574.
24 Lee, W.-C.C., Wang, D.-S., Zhu, Y., and Zhang, X.P. (2023). *Nat. Chem.* 15: 1569–1580.
25 Naruta, Y., Tani, F., and Maruyama, K. (1990). *J. Chem. Soc. Chem. Commun.* 1378–1380.
26 Naruta, Y., Tani, F., and Maruyama, K. (1991). *Tetrahedron: Asymmetry* 2: 533–542.
27 Mahammed, A. and Gross, Z. (2005). *J. Am. Chem. Soc.* 127: 2883–2887.
28 Groves, J.T. and Viski, P. (1989). *J. Am. Chem. Soc.* 111: 8537–8538.
29 Wang, H.-H., Shao, H., Huang, G. et al. (2023). *Angew. Chem. Int. Ed.* 62: e202218577.
30 Sessler, J.L. and Seidel, D. (2003). *Angew. Chem. Int. Ed.* 42: 5134–5175.
31 Rose, E., Andrioletti, B., Zrig, S., and Quelquejeu-Etheve, M. (2005). *Chem. Soc. Rev.* 34: 573–583.
32 Chen, Z. and Yin, G. (2015). *Chem. Soc. Rev.* 44: 1083–1100.
33 Barona-Castano, J.C., Carmona-Vargas, C.C., Brocksom, T.J., and de Oliveira, K.T. (2016). *Molecules* 21: 310.
34 Huang, X. and Groves, J.T. (2017). *J. Biol. Inorg. Chem.* 22: 185–207.
35 Pereira, M.M., Dias, L.D., and Calvete, M.J.F. (2018). *ACS Catal.* 8: 10784–10808.
36 Singh, R. and Mukherjee, A. (2019). *ACS Catal.* 9: 3604–3617.
37 Weissenborn, M.J. and Koenigs, R.M. (2020). *ChemCatChem* 12: 2171–2179.
38 Ahmad, I. and Shagufta, S.R. (2022). *Tetrahedron* 104: 132604.
39 Xiao, X., Xu, K., Gao, Z.-H. et al. (2023). *Sci. China Chem.* 66: 1553–1633.
40 Prier, C.K., Zhang, R.K., Buller, A.R. et al. (2017). *Nat. Chem.* 9: 629–634.
41 Yang, Y., Cho, I., Qi, X. et al. (2019). *Nat. Chem.* 11: 987–993.
42 Jia, Z.J., Gao, S., and Arnold, F.H. (2020). *J. Am. Chem. Soc.* 142: 10279–10283.
43 Athavale, S.V., Gao, S., Liu, Z. et al. (2021). *Angew. Chem. Int. Ed.* 60: 24864–24869.
44 Athavale, S.V., Gao, S., Das, A. et al. (2022). *J. Am. Chem. Soc.* 144: 19097–19105.
45 Liu, Z., Qin, Z.-Y., Zhu, L. et al. (2022). *J. Am. Chem. Soc.* 144: 80–85.
46 Mai, B.K., Neris, N.M., Yang, Y., and Liu, P. (2022). *J. Am. Chem. Soc.* 144: 11215–11225.
47 Gao, S., Das, A., Alfonzo, E. et al. (2023). *J. Am. Chem. Soc.* 145: 20196–20201.
48 Zhang, J., Huang, X., Zhang, R.K., and Arnold, F.H. (2019). *J. Am. Chem. Soc.* 141: 9798–9802.
49 Zhang, R.K., Chen, K., Huang, X. et al. (2019). *Nature* 565: 67–72.
50 Zhou, A.Z., Chen, K., and Arnold, F.H. (2020). *ACS Catal.* 10: 5393–5398.
51 Brandenberg, O.F., Prier, C.K., Chen, K. et al. (2018). *ACS Catal.* 8: 2629–2634.
52 Chen, K., Zhang, S.-Q., Brandenberg, O.F. et al. (2018). *J. Am. Chem. Soc.* 140: 16402–16407.
53 Knight, A.M., Kan, S.B.J., Lewis, R.D. et al. (2018). *ACS Cent. Sci.* 4: 372–377.
54 Carminati, D.M. and Fasan, R. (2019). *ACS Catal.* 9: 9683–9697.
55 Chen, K. and Arnold, F.H. (2020). *J. Am. Chem. Soc.* 142: 6891–6895.

56 Suzuki, K., Shisaka, Y., Stanfield, J.K. et al. (2020). *Chem. Commun.* 56: 11026–11029.

57 Porter, N.J., Danelius, E., Gonen, T., and Arnold, F.H. (2022). *J. Am. Chem. Soc.* 144: 8892–8896.

58 Mao, R., Wackelin, D.J., Jamieson, C.S. et al. (2023). *J. Am. Chem. Soc.* 145: 16176–16185.

59 Chen, K., Huang, X., Kan, S.B.J. et al. (2018). *Science* 360: 71–75.

60 Cho, I., Prier, C.K., Jia, Z.J. et al. (2019). *Angew. Chem. Int. Ed.* 58: 3138–3142.

61 Cui, H.-B., Xie, L.-Z., Wan, N.-W. et al. (2019). *Green Chem.* 21: 4324–4328.

62 Xie, L., Chen, K., Cui, H. et al. (2020). *ChemBiochem* 21: 1820–1825.

63 Steck, V., Carminati, D.M., Johnson, N.R., and Fasan, R. (2020). *ACS Catal.* 10: 10967–10977.

64 Goldberg, N.W., Knight, A.M., Zhang, R.K., and Arnold, F.H. (2019). *J. Am. Chem. Soc.* 141: 19585–19588.

65 Huang, X., Garcia-Borras, M., Miao, K. et al. (2019). *ACS Cent. Sci.* 5: 270–276.

66 Miller, D.C., Lal, R.G., Marchetti, L.A., and Arnold, F.H. (2022). *J. Am. Chem. Soc.* 144: 4739–4745.

67 Zhou, Q., Chin, M., Fu, Y. et al. (2021). *Science* 374: 1612–1616.

68 Rui, J., Zhao, Q., Huls, A.J. et al. (2022). *Science* 376: 869–874.

69 Roy, S., Vargas, D.A., Ma, P. et al. (2023). *Nat. Catal.* 7: 65–76.

70 Meunier, B., de Visser, S.P., and Shaik, S. (2004). *Chem. Rev.* 104: 3947–3980.

71 Poulos, T.L. (2014). *Chem. Rev.* 114: 3919–3962.

72 Cook, D.J., Finnigan, J.D., Cook, K. et al. (2016). *Advances in Protein Chemistry and Structural Biology*, vol. 105, 105–126. Elsevier Ltd.

73 Hammer, S.C., Knight, A.M., and Arnold, F.H. (2017). *Curr. Opin. Green Sustain. Chem.* 7: 23–30.

74 Fasan, R., Jennifer Kan, S.B., and Zhao, H. (2019). *ACS Catal.* 9: 9775–9788.

75 Guo, M., Corona, T., Ray, K., and Nam, W. (2019). *ACS Cent. Sci.* 5: 13–28.

76 Hanefeld, U., Hollmann, F., and Paul, C.E. (2022). *Chem. Soc. Rev.* 51: 594–627.

77 Sibi, M.P. and Porter, N.A. (1998). *Acc. Chem. Res.* 32: 163–171.

78 Sibi, M.P., Manyem, S., and Zimmerman, J. (2003). *Chem. Rev.* 103: 3263–3296.

79 Mondal, S., Dumur, F., Gigmes, D. et al. (2022). *Chem. Rev.* 122: 5842–5976.

80 Wang, F., Chen, P., and Liu, G. (2018). *Acc. Chem. Res.* 51: 2036–2046.

81 Wang, K. and Kong, W. (2018). *Chin. J. Chem.* 36: 247–256.

82 Gu, Q.-S., Li, Z.-L., and Liu, X.-Y. (2019). *Acc. Chem. Res.* 53: 170–181.

83 Li, Z.-L., Fang, G.-C., Gu, Q.-S., and Liu, X.-Y. (2020). *Chem. Soc. Rev.* 49: 32–48.

84 Genzink, M.J., Kidd, J.B., Swords, W.B., and Yoon, T.P. (2022). *Chem. Rev.* 122: 1654–1716.

85 Nagib, D.A. (2022). *Chem. Rev.* 122: 15989–15992.

86 Yao, W., Bergamino, E.A.B., and Ngai, M.Y. (2022). *ChemCatChem* 14: e202101292.

87 Yang, C.-J., Liu, L., Gu, Q.-S., and Liu, X.-Y. (2024). *CCS Chem.* 6: 1612–1627.

88 Liu, C., Liu, D., and Lei, A. (2014). *Acc. Chem. Res.* 47: 3459–3470.

89 Liu, C., Yuan, J., Gao, M. et al. (2015). *Chem. Rev.* 115: 12138–12204.

90 Yang, Y., Lan, J., and You, J. (2017). *Chem. Rev.* 117: 8787–8863.
91 Egami, H., Matsumoto, K., Oguma, T. et al. (2010). *J. Am. Chem. Soc.* 132: 13633–13635.
92 Narute, S., Parnes, R., Toste, F.D., and Pappo, D. (2016). *J. Am. Chem. Soc.* 138: 16553–16560.
93 Tkachenko, N.V., Lyakin, O.Y., Samsonenko, D.G. et al. (2018). *Catal. Commun.* 104: 112–117.
94 Horibe, T., Nakagawa, K., Hazeyama, T. et al. (2019). *Chem. Commun.* 55: 13677–13680.
95 Ding, K., Li, X., Ji, B. et al. (2005). *Curr. Org. Synth.* 2: 499–545.
96 Dyadyuk, A., Vershinin, V., Shalit, H. et al. (2022). *J. Am. Chem. Soc.* 144: 3676–3684.
97 Fritsche, R.F., Schuh, T., Kataeva, O., and Knölker, H.J. (2023). *Chem. Eur. J.* 29: e202203269.
98 Oguma, T. and Katsuki, T. (2012). *J. Am. Chem. Soc.* 134: 20017–20020.
99 Narute, S. and Pappo, D. (2017). *Org. Lett.* 19: 2917–2920.
100 Surgenor, R.R., Liu, X., Keenlyside, M.J.H. et al. (2022). *Nat. Chem.* 15: 357–365.
101 Li, Z., Cao, L., and Li, C.-J. (2007). *Angew. Chem. Int. Ed.* 46: 6505–6507.
102 Tanaka, T., Hashiguchi, K., Tanaka, T. et al. (2018). *ACS Catal.* 8: 8430–8440.
103 Xu, N., Pu, M., Yu, H. et al. (2024). *Angew. Chem. Int. Ed.* 63: e202314256.
104 Jin, M., Adak, L., and Nakamura, M. (2015). *J. Am. Chem. Soc.* 137: 7128–7134.
105 Sharma, A.K., Sameera, W.M.C., Jin, M. et al. (2017). *J. Am. Chem. Soc.* 139: 16117–16125.
106 Lee, W., Zhou, J., and Gutierrez, O. (2017). *J. Am. Chem. Soc.* 139: 16126–16133.
107 Youshaw, C.R., Yang, M.-H., Gogoi, A.R. et al. (2023). *Org. Lett.* 25: 8320–8325.
108 Iwamoto, T., Okuzono, C., Adak, L. et al. (2019). *Chem. Commun.* 55: 1128–1131.
109 Liu, G.-S., Zhang, Y.-Q., Yuan, Y.-A., and Xu, H. (2013). *J. Am. Chem. Soc.* 135: 3343–3346.
110 Li, H., Shen, S.-J., Zhu, C.-L., and Xu, H. (2018). *J. Am. Chem. Soc.* 140: 10619–10626.
111 Ge, L., Zhou, H., Chiou, M.-F. et al. (2020). *Nat. Catal.* 4: 28–35.
112 Lv, D., Sun, Q., Zhou, H. et al. (2021). *Angew. Chem. Int. Ed.* 60: 12455–12460.
113 Wang, K., Li, Y., Li, X. et al. (2021). *Org. Lett.* 23: 8847–8851.
114 Liu, W., Pu, M., He, J. et al. (2021). *J. Am. Chem. Soc.* 143: 11856–11863.
115 Wang, R., Wang, C.-Y., Liu, P. et al. (2023). *Sci. Adv.* 9: eadh5195.
116 Luo, L., Zhang, X., Huang, C., and Lian, Z. (2024). *Org. Chem. Front.* 11: 1678–1684.
117 Nakanishi, M., Salit, A.F., and Bolm, C. (2008). *Adv. Synth. Catal.* 350: 1835–1840.
118 Steinlandt, P.S., Hemming, M., Xie, X. et al. (2023). *Chem. Eur. J.* 29: e202300267.
119 Cui, T., Ye, C.X., Thelemann, J. et al. (2023). *Chin. J. Chem.* 41: 2065–2070.